Cyclonic gyre in the tropical South Atlantic

ARNOLD L. GORDON* and KATHRYN T. BOSLEY*

Abstract—A cyclonic gyre within the eastern tropical South Atlantic is resolved by an extensive oceanographic station array obtained in 1983 and 1984. The gyre is centered near 13°S and 5°E with a sea surface relief relative to 1500 decibars (db) of 8 dyn cm. The 500 db surface relative to 1500 db reveals a much diminished cyclonic circulation, shifted slightly to the south. The weak baroclinic expression of the cyclonic gyre is confined for the most part to the upper 300 db, with a surface characteristic speed of only 3 cm s^{-1}. A transport of 5×10^6 m^3 s^{-1} across a line from the gyre center to the African continental margin, including the Angola Current, may best depict the gyre 0–300 db transport (relative to 1500 db). Ship drift data for the region do not show the presence of the cyclonic gyre because the wind-induced Ekman layer masks the gyre. The thermocline of the cyclonic gyre is significantly saltier and lower in oxygen than the suspected source water: the main thermocline of the South Atlantic subtropical gyre. A strong front near 18°S, the Angola–Benguela Front, separates the cyclonic gyre regime from that of the subtropical gyre. Using the regional freshwater balance, gyre thermocline residence time is determined to be between 4.4 and 8.5 years, implying an oxygen utilization of 0.3–0.5 ml l^{-1} y^{-1}. Below the thermocline there is some evidence for southward flow of North Atlantic Deep Water along the eastern boundary. It is inferred that this flow is fed by eastward spreading of North Atlantic Deep Water along the equatorial belt.

INTRODUCTION

BASIN-SCALE maps of the sea surface dynamic height relative to an assumed zero flow reference level at depth (DEFANT, 1961, his Fig. 271; REID *et al.*, 1977; TSUCHIYA, 1985) reveal eastward geostrophic flow between the equator and 10°S in the South Atlantic Ocean. This current extends from 20°W to the African continent. The zonal currents across the Greenwich Meridan simulated by a multi-level wind-driven numerical model exhibit eastward flow below a shallow westward-flowing surface layer for the same region (PHILANDER and PACANOWSKI, 1986, see their Fig. 17).

The large-scale dynamic topography maps mentioned above do not resolve the sea level slope along the eastern boundary, and hence do not determine whether the flow reaching the African coast turns northward into the Gulf of Guinea or to the south. Current profiler measurements taken over the continental shelf and upper slope from Port Gentil (1°S) to Pointe Noire (5°S; WACONGNE, 1988) show evidence of a weak, poleward-flowing undercurrent, somewhat stronger during the summer months. A connection between the eastward-flowing South Equatorial Countercurrent and the southward-flowing coastal undercurrent can be inferred from the hydrographic data of the May 1973 cruise of the R.V. *Capricorne* (WACONGNE, 1988, her Fig. 31a). Detailed maps of dynamic height

---

*Lamont-Doherty Geological Observatory of Columbia University, Palisades, NY 10964, U.S.A.

constructed for the Gulf of Guinea indicate southward flow along the coast of Angola from 10° to 20°S (MERLE, 1978). Surface temperature maps (MAZEIKA, 1968; HASTENRATH and LAMB, 1977) show southward displacement of warm water to at least 15°S along the African coast, supporting the view that the eastward flow turns southward upon reaching the African Coast.

A cyclonic gyre in the eastern tropical South Atlantic was first discussed in detail by MOROSHKIN et al. (1970) using an April to June 1968 oceanographic station array. The dynamic topography maps resulting from that survey show cyclonic motion to 300 m depth, centered near 14°S and 4°E, relative to 1000 decibars (db). Geostrophic velocities within the cyclonic gyre do not exceed 3 cm s^{-1}. They make reference to, but do not elaborate upon, an opposing, shallow, wind-driven surface layer.

The western boundary of the cyclonic gyre is marked by the broad sweep of surface flow towards the northwest stretching across the South Atlantic, as seen on the large-scale dynamic topography maps. The northern and eastern limbs of the cyclonic gyre have been discussed separately by various authors. The eastward-flowing northern limb is referred to as the South Equatorial Countercurrent (REID, 1964; MOLINARI et al., 1981; MOLINARI, 1982). Molinari, using hydrographic data obtained during four cruises from July 1978 to March 1980, made a distinction between two bands of eastward flow: (1) the South Equatorial Undercurrent located between 3° and 5°S with a subsurface maximum speed of 40 cm s^{-1} and a transport ranging from 5 to 23 × 10^6 m^3 s^{-1} (Sv) (relative to 1000 db); and (2) the South Equatorial Countercurrent located between 7° and 9°S with maximum speed of 10 cm s^{-1} and a transport range from 3 to 7 Sv.

The Angola Current (CURRIE, 1953) forms the eastern boundary of the gyre. This current carries equatorial water southward to the vicinity of Cape Frio, 15° to 18°S, where it encounters the cold, northward-flowing Benguela Current. The confluence of these two currents causes a sharp thermal front, called the Angola–Benguela Front, in the upper 50 m, along with a highly variable circulation pattern (HART and CURRIE, 1960; SHANNON, 1985; SHANNON et al., 1987). A narrow filament of the Benguela water may extend north to 12°S before returning south immediately west of the Angola Current (MOROSHKIN et al., 1970). It is possible that the position of the front is set by the shelf width or change of the orientation of the coastline, though change in wind stress also has been suggested (SHANNON et al., 1987). Seasonal variations in the position of the Angola–Benguela Front seem to be associated with the wind field, and there is evidence of El Niño-like episodes in the South Atlantic in which warm surface water extends further south along the Angola coast, suppressing Benguela upwelling (SHANNON et al., 1987). These events are also associated with more westward penetration of the Agulhas Retroflection (SHANNON et al., 1986). Warm events occurred in the years 1963 and 1984, the first such appearances since the early 1950s (SHANNON et al., 1986). Anomalous warming of the eastern tropical South Atlantic during the 1984 episode is clearly shown in the June 1984 vs the June 1983 satellite-derived sea surface temperature images appearing on the cover of Eos (LEGECKIS, 1989).

An XBT section obtained in May 1987 from the R.R.S. Discovery (Fig. 1) provides a detailed thermal view of a meridional slice across this gyre. The 12°C isotherm reaches its shallowest depth of 150 m near 12–13°S, with a secondary shallowing near 4°–5°S, while the 10°C isotherm attains its shallowest depth of approximately 250 m near 18°S. The double-peaked 12°C isotherm is consistent with the two axes of eastward current mentioned by MOLINARI (1982). The poleward shift of the 10°C isotherm crest, relative to that of the 12°C
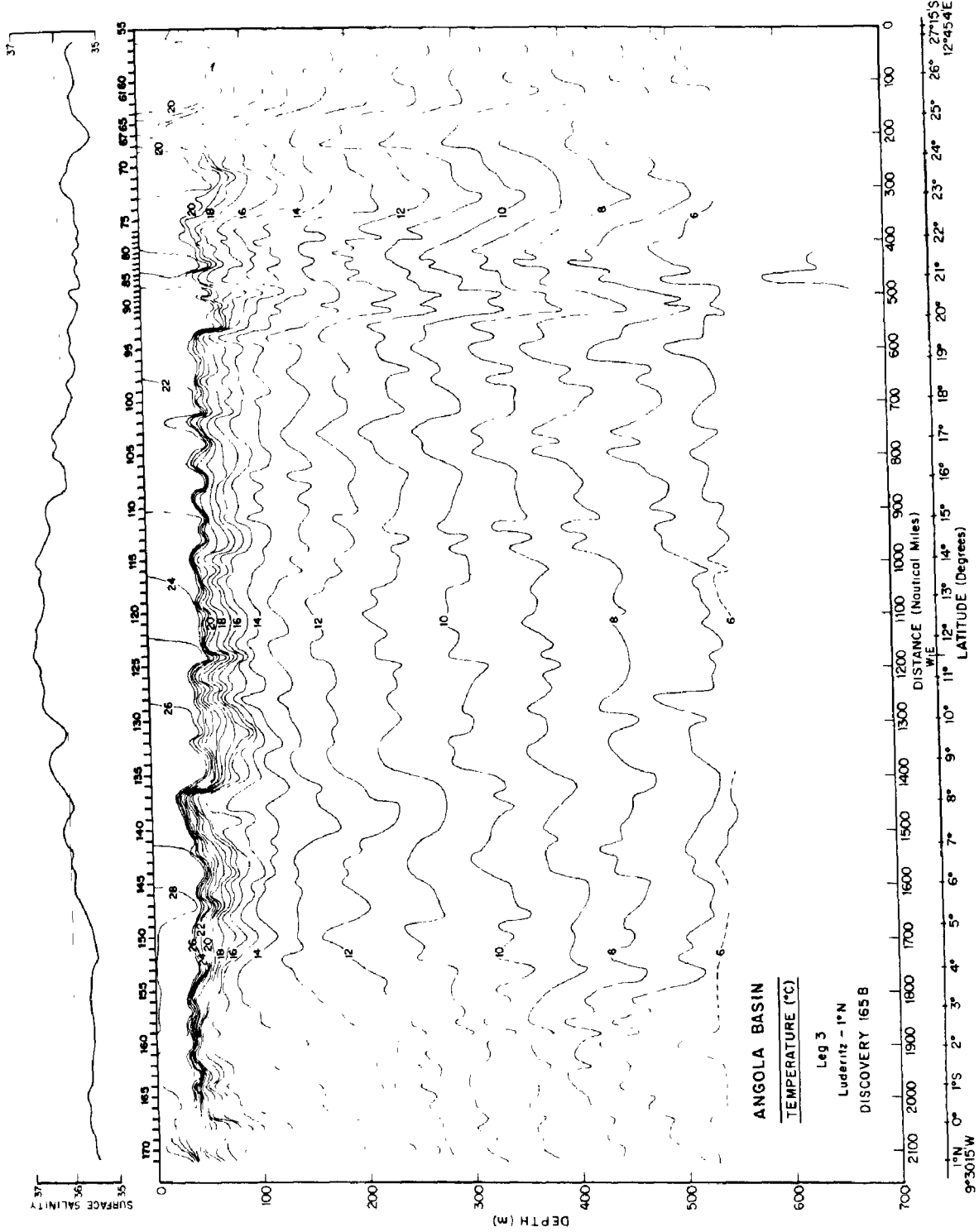
Fig. 1. Temperature for the upper 700 m with surface salinity, obtained by XBT and surface sampling in May 1987 from the R.R.S *Discovery*. The section extends from near Luderitz (~27°S, ~12°E) to Liberia (1°N, ~10°W) (see Fig. 2).

isotherm, reflects a similar shift of the cyclonic gyre observed in the dynamic topography pattern, discussed below. The surface salinity distribution along the XBT track (Fig. 1) shows high values within the cyclonic gyre. The gyre's high surface salinity characteristic is matched by high salinity throughout the thermocline stratum.

HASTENRATH and MERLE (1987) compiled historical hydrographic data between 8°W and 8°E and north of 20°S in order to construct seasonal meridional temperature sections. They show a crest in the 12–14°C isotherms near 10°S throughout the year, though somewhat weaker in July to September. The "Angola Dome", a cold water feature at the 20 m horizon, centered near 10°S, 8°E, has been defined by MAZEIKA (1967) using data collected from 1902 to 1963. This feature is not evident in the July to September period.

In summary, there is evidence for a weak cyclonic gyre in the eastern tropical South Atlantic Ocean, possibly weaker during the southern hemisphere winter. An extensive South Atlantic oceanographic data set obtained during 1983 and 1984 allows further inspection of this gyre. We use this data set to better resolve the gyre configuration and discuss its characteristics. We first discuss the relative geostrophic circulation and the wind-induced Ekman layer flow and Sverdrup transport patterns. We then discuss the water mass characteristics of the cyclonic gyre.

THE 1983–1984 DATA SET

During 1983 and 1984 there were a number of oceanographic expeditions to the South Atlantic (Fig. 2; Table 1). The oceanographic stations are clustered in the eastern and western troughs of the South Atlantic; however, two R.V. *Oceanus* sections provide some zonal continuity. The data in the northeast part of the domain include stations obtained in both 1983 and 1984, hence the developing thermal anomaly of 1984 may induce some degree of non-synopticity. However, the existence of the cyclonic gyre in April to June 1968 (MOROSHKIN *et al.*, 1970), which was not identified as an anomalous period by SHANNON *et al.* (1986) and the presence of a cold dome in the historical data set compiled by HASTENRATH and MERLE (1987) and in the 1987 XBT section (Fig. 1), indicate the gyre is a quasi-stationary climatic feature.

BAROCLINIC MASS FIELD

Sea surface and 500 db relative dynamic topography

The dynamic height of the sea surface relative to 1500 db highlights several interesting features about the circulation in the South Atlantic during 1983–1984 (Fig. 3a). A reference level of 1500 db is used to inspect the baroclinic geostrophic flow in order to incorporate shallow features on the continental slope. Previously described features, such as the Angola and Benguela Currents, the Agulhas Retroflection south of Africa and subtropical anticyclonic gyre (axis near 25°S in the west and 32°S in the east), are evident in the 1983–1984 dynamic topography pattern. The cyclonic gyre is centered near 13°S, 5°E and has an approximate relief of 8 dyn cm. While it is not obvious where to draw the western boundary, using the 1.55 dyn m contour the gyre is nearly circular with a characteristic diameter of 2000 km. The cyclonic feature appears on the 500 db surface (500/1500 db; Fig 3b) but it is weaker and centered slightly further south, near 18°S.
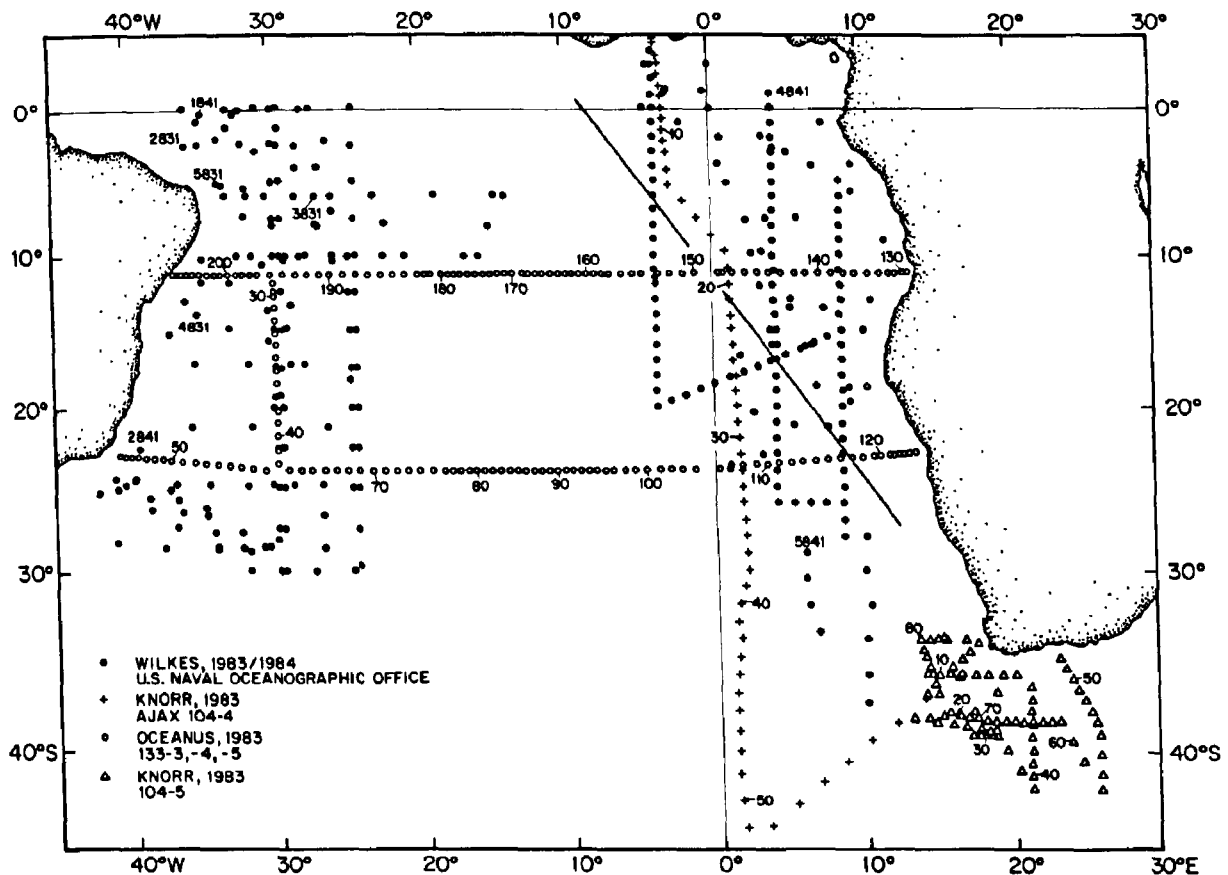
Fig. 2. Station map of the 1983–1984 oceanographic data set used in this study (see Table 1). The position of the 1987 XBT section shown in Fig. 1 is indicated as a solid line.

Geostrophic velocity and transport

The characteristic values of surface geostrophic velocity relative to 1500 db vary between 2 and 4 cm s^{-1} within the gyre with a weak velocity maximum at 50 m (Fig. 4). The average velocity profiles of WACONGNE (1988, her Fig. 40) off the coast of Gabon display striking similarities to those in Fig. 4. A mean southward flow of about 8 cm s^{-1} extends to a depth of 300 m, below a shallow northward surface flow. Both the geostrophic and directly measured current profiles reveal a reversal of flow below 300 m. The near-surface circulation pattern is relatively insensitive to choice of reference level. Surface velocities change by only 20% and the direction of the flow is not altered as the reference level is lowered to 3000 db (Fig. 4).

Table 1. Oceanographic expeditions to the South Atlantic

Ship	Dates	Area covered
U.S.N.S. *Wilkes*	Mar. 1983–Nov. 1984	Western and eastern South Atlantic
R.V. *Oceanus*	Feb.–Mar. 1983	Zonal sections along 11° and 24°S
R.V. *Knorr**	Oct.–Nov. 1983	Along the Greenwich Meridian from 5°N to 45°S
R.V. *Knorr*	Nov.–Dec. 1983	Agulhas Retroflection region (CAMP *et al.*, 1986)

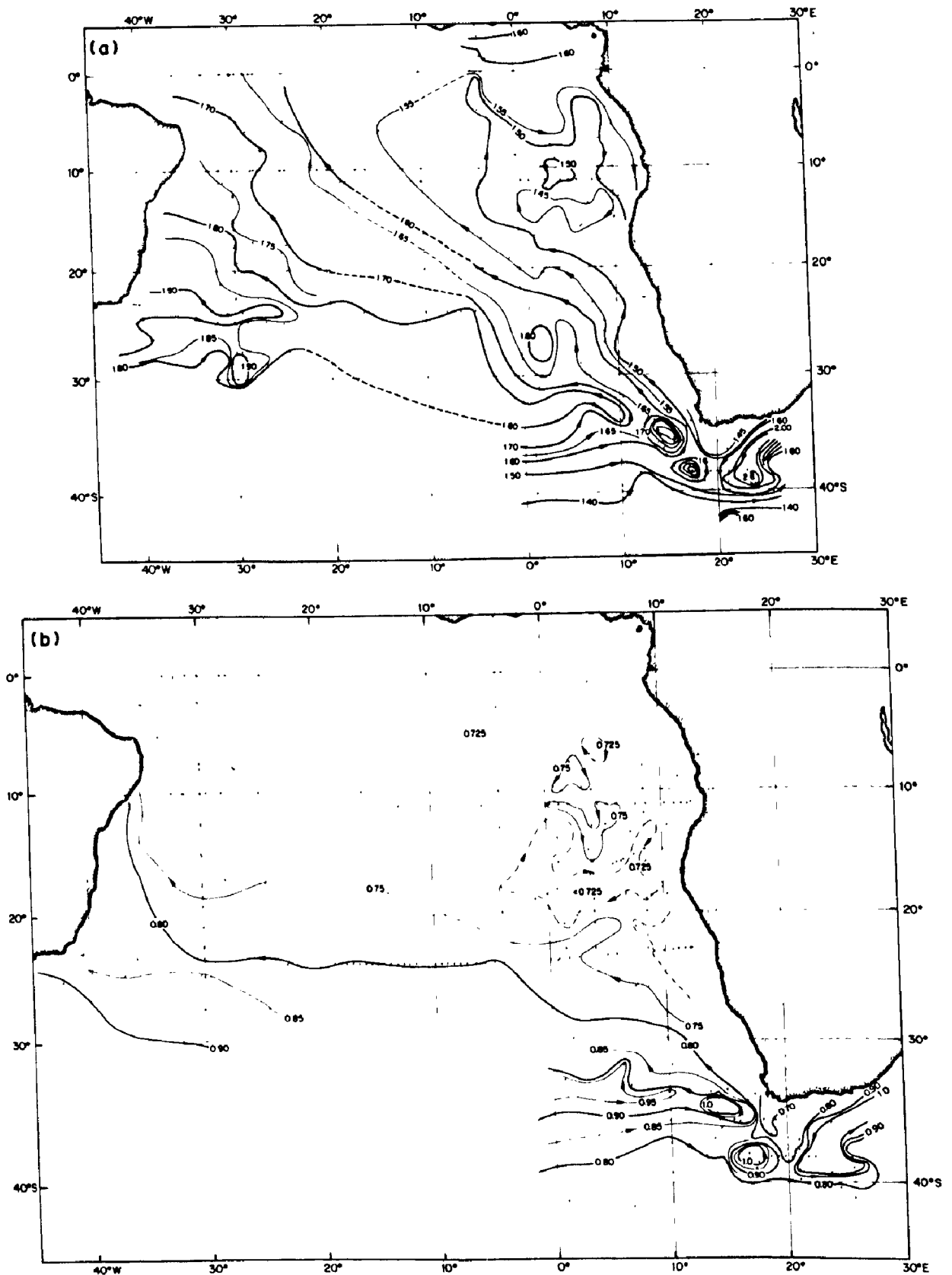*Ajax expedition (SIO, 1985).

Fig. 3.   (a) Dynamic topography of the sea surface relative to the 1500 db surface. (b) Dynamic
topography of the 500 db surface relative to the 1500 db surface.

Baroclinic transport relative to 1500 db, for the ocean stratum from the sea surface to 300 db, was determined between station pairs radiating from the gyre center (Fig. 5). Spatial variability of the transport is evident with an average of 3.8 Sv and a standard deviation of 1.4 Sv. The 212–132 station pair best covers the full extent of the gyre, since it is well bounded, extending from the gyre center to the African continental margin. That it reveals a relatively large transport, 4.5 Sv, suggests that the other station pairs, ending in mid-ocean, may not be recording the full gyre. This is particularly evident for the western pairs, because of the diffuse western rim of the gyre, and for the northern pairs which do not include possible equatorial current contributions. The 14 month separation of Stas 212 and 132 spans the warm event mentioned above and hence introduces an element of non-synopticity. However, station pair 212–307, both obtained in 1984 (but in opposite seasons), also yields a large transport of 5.6 Sv. It is suggested that the characteristic transport may be taken as 5 Sv. The maximum transport of 6.5 Sv occurs across a station pair which extends into the Benguela Current, south of the cyclonic gyre.

Since the geostrophic velocities are small and the Coriolis parameter is weak at the low latitudes of the gyre, it is appropriate to evaluate the accuracy of these geostrophic determinations. One can access the accuracy of the geostrophic method by comparison to
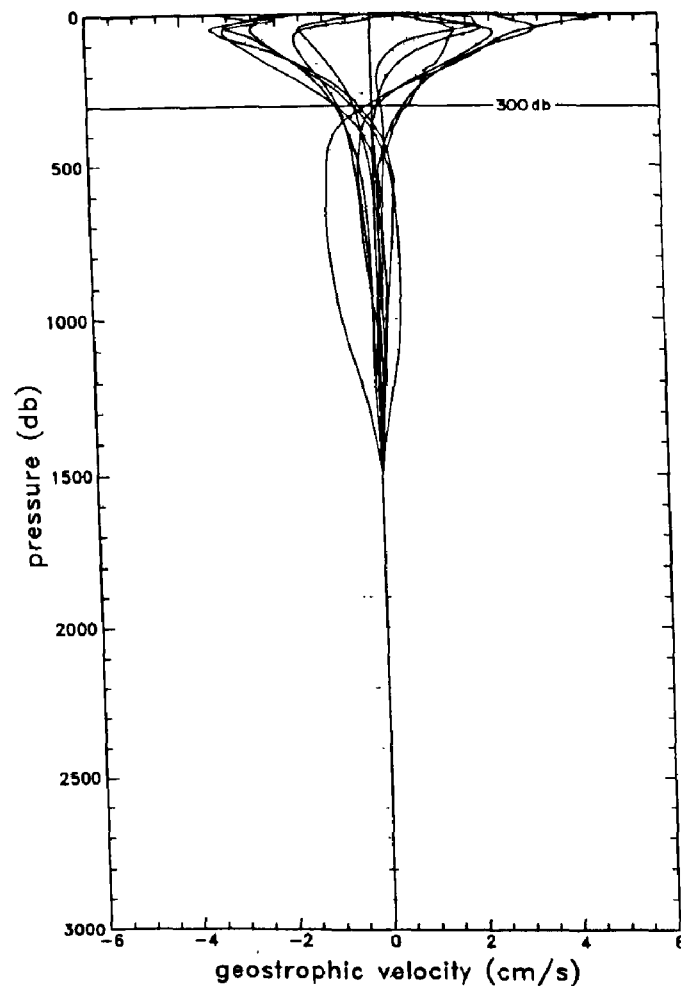

Fig. 4.   Geostrophic velocity (cm s^{-1}) vs pressure for the station pairs pictured in Fig. 5. The geostrophic velocity component perpendicular to the station pairs are shown. Values using a 1500 db reference level are solid lines, while those using a 3000 db reference are dotted.
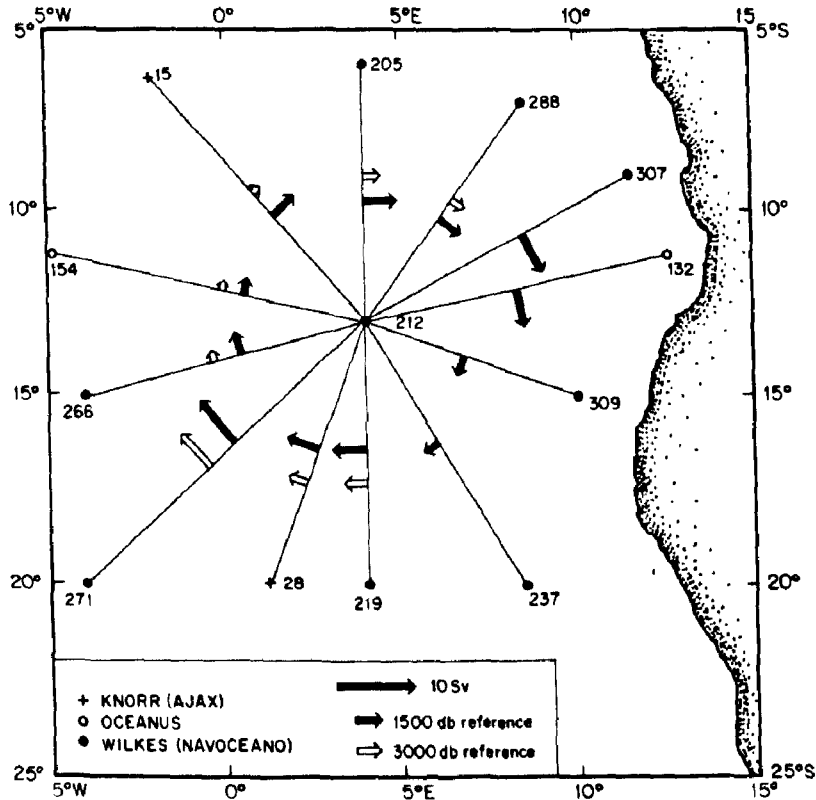
Fig. 5. Map of the transport between the surface and 300 db referenced to 1500 db. Values using a 1500 db reference level are solid, while those using a 3000 db reference level are open. The eastern stations do not extend to 3000 db. Station dates: 132, 154 (*Oceanus*)—March 1983; 15, 28 (*Knorr*)—October 1983; 205, 212, 219, 237 (*Wilkes*)—May 1984; 266, 271 (*Wilkes*)—June 1984; 288 (*Wilkes*)—July 1984; 307, 309 (*Wilkes*)—November 1984.

directly measured currents. WÜST (1924), SWALLOW (1971) and HORTON and STURGES (1979) have followed this approach. The comparisons of HORTON and STURGES (1979) of geostrophic shear deduced from MODE STD hydrographic casts with shear measurements from current meters, show an r.m.s. difference of 0.4–1.9 cm s^{-1} in speed and 0.32–0.42 radians in direction. GORDON (1965) investigated errors in geostrophic calculations stemming from salinity, temperature and navigational errors. He finds that the error accumulates with distance from the reference level. Using a 1500 db reference level, the surface speed uncertainty at the 90% confidence level, for the latitudes of the cyclonic gyre is approximately 2 cm s^{-1}. Therefore, it is concluded that the directional sense of the upper 300 db of the cyclonic gyre is significant but that the speeds approach the accuracy of the method.

WIND FORCING

Ekman layer circulation

The PHILANDER and PACANOWSKI (1986) model shows that the eastward flow marking the northern rim of the cylonic gyre does not have an expression at the sea surface. Supporting this is ship drift information which reveals westward flow (RICHARDSON and WALSH, 1986; ARNAULT, 1987; RICHARDSON and PHILANDER, 1987; RICHARDSON, 1988)

across the entire region of the cyclonic gyre. The most likely explanation is that wind-induced movement within the Ekman layer reverses the rather weak near-surface geostrophic current.

The LEVITUS (1982) gridded data set shows the surface cyclonic circulation (Fig. 6a). There are three longitudes of northward flow, 0°, 10°W and 20°–30°W, the latter may be taken as the western rim of the cyclonic gyre. Averaged gridded data tend to diminish the magnitude of the current and essentially remove boundary currents.

Using the mean annual gridded wind stress data set (HELLERMAN and ROSENSTEIN, 1983), the surface water movement, following the Ekman spiral formulation (45° to left of the wind in the southern hemisphere), and using an effective viscosity coefficient $A_z = 0.01$ $m^2 s^{-1}$ (PRICE et al., 1987), yields a pattern of surface flow (Fig. 6b) more vigorous than the geostrophic field, and directed towards the northwest across the full extent of the cyclonic gyre. Vectorally combining the 0/1500 db geostrophic surface circulation from Fig. 6a with the Ekman surface flow of Fig. 6b shows the dominance of the wind-induced surface flow (Fig. 6c). A surface Ekman velocity for $A_z = 0.01$ $m^2 s^{-1}$ which is at the upper bound of the range given by POND and PICKARD (1983), yields smaller wind-induced surface flow, allowing some influence of the surface geostrophic cyclonic gyre circulation to emerge (Fig. 6d). Using a 50 m thick Ekman slab model slightly alters the composite surface circulation pattern, but does not allow the cyclonic gyre to surface.

RICHARDSON's (1988) ship drift map reveals northwest flow throughout the region of the cyclonic gyre. However, it shows significantly lower speeds near 10°S east of 10°W. Perhaps the gyre's geostrophic flow exerts some influence on the surface flow.

Sverdrup gyre circulation

Negative wind stress curl predominates over the region of the cyclonic gyre (Fig. 7a), which drives cyclonic circulation according to the Sverdrup model (SVERDRUP, 1947). The zero wind stress curl isopleth follows the northern edge of the strong geostrophic flow towards the northwest (Fig. 6a). The Sverdrup mass transport function is integrated along a line of latitude from the eastern side of the ocean in order to map the mass transport streamfunction (Fig. 7b). The Sverdrup transport pattern reveals cyclonic circulation in the tropical South Atlantic, with an integrated transport at the western boundary between near the equator and 10°S of 5–10 Sv. Approximately 10% higher transport is calculated at the position of the zero wind stress curl isopleth, about 400 km off the western margin. These transport values are similar to those calculated from the 1983–1984 data set, though the strong eastern shift of the cyclonic gyre center evident in the dynamic topography map is not present in the Sverdrup mass transport streamfunction pattern.

STRATIFICATION AND WATER MASS CHARACTERISTICS

Surface and thermocline

The Ajax section along approximately the Greenwich Meridian and the R.V. Oceanus section along 11°S (Fig. 2) form useful meridional and zonal views of the cyclonic gyre. The Ajax section from 2°S (Sta. 10) to 22°S (Sta. 30) includes the cyclonic gyre and the Benguela Current limb of the subtropical gyre to the south. The R.V. Oceanus section extends from the Angola Current marking the eastern branch of the cyclonic gyre, across the cyclonic gyre into the western South Atlantic. The potential temperature vs salinity
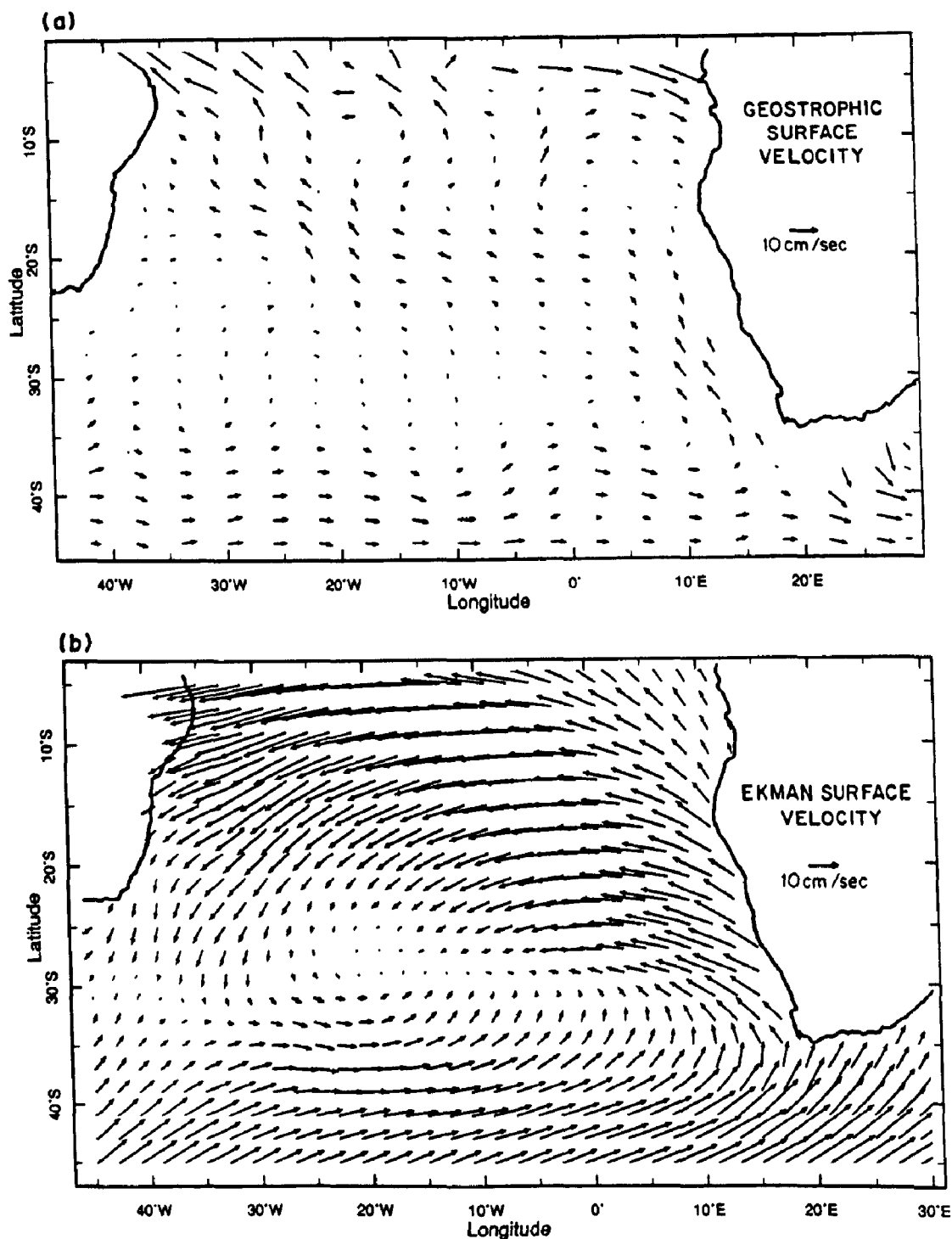
Fig. 6. (a) Mean annual geostrophic surface velocity (referenced to 1500 db) using Levitus (1982) gridding of the historical hydrographic data. (b) Ekman surface flow using mean annual wind stress vectors from Hellerman and Rosenstein (1983) in the Ekman spiral formulation with $A_z = 0.01$ m^2 s^{-1}. (c) Vectorally combined geostrophic (a) and Ekman flow with $A_z = 0.01$ m^2 s^{-1} (b). (d) Vectorally combined geostrophic and Ekman flow with $A_z = 0.1$ m^{2}s^{-1}.

(c)

EKMAN +
GEOSTROPHIC
VELOCITY

classic form + 0/1500 db

10 cm/sec

(d)

EKMAN +
GEOSTROPHIC
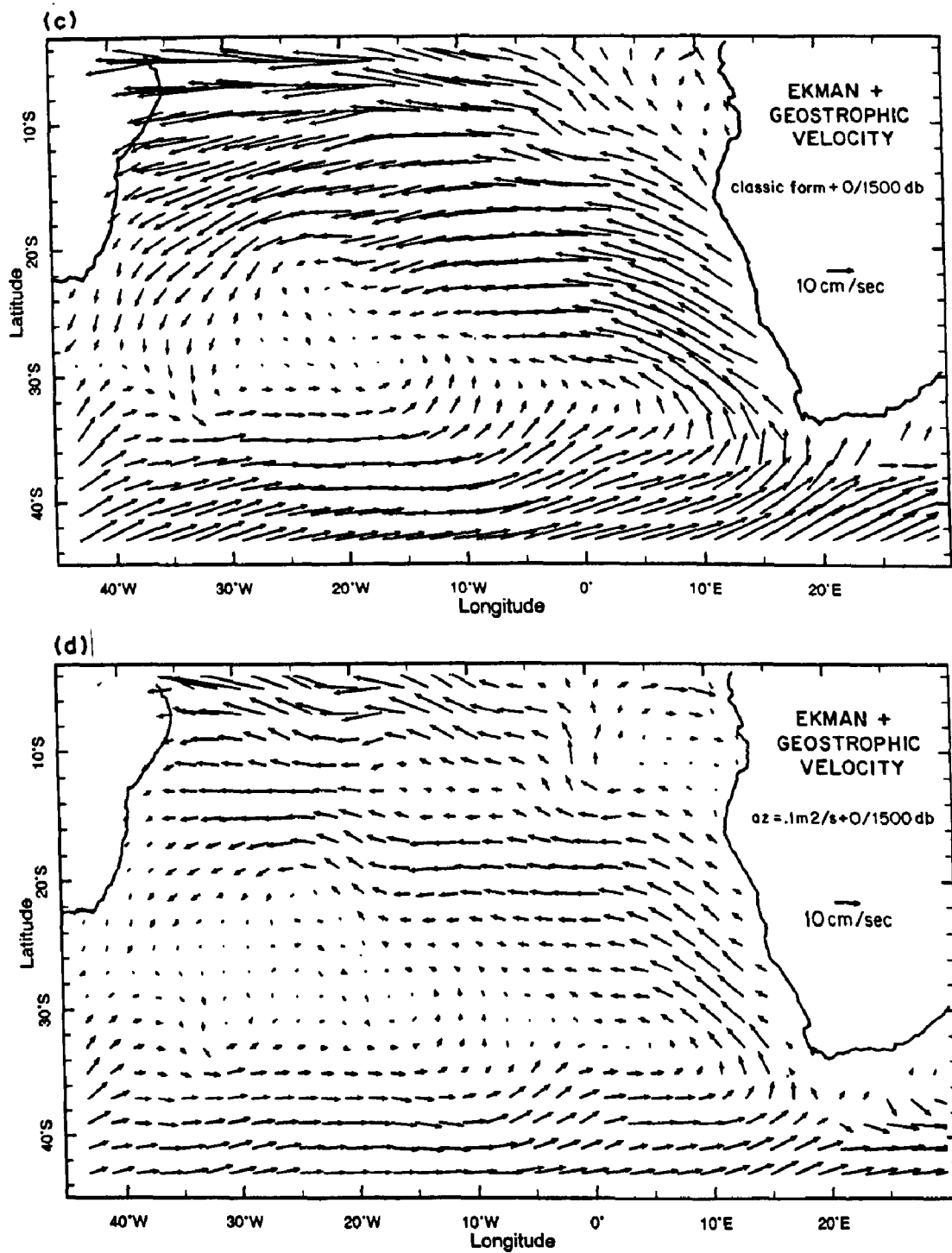VELOCITY

az = .1m2/s + 0/1500 db
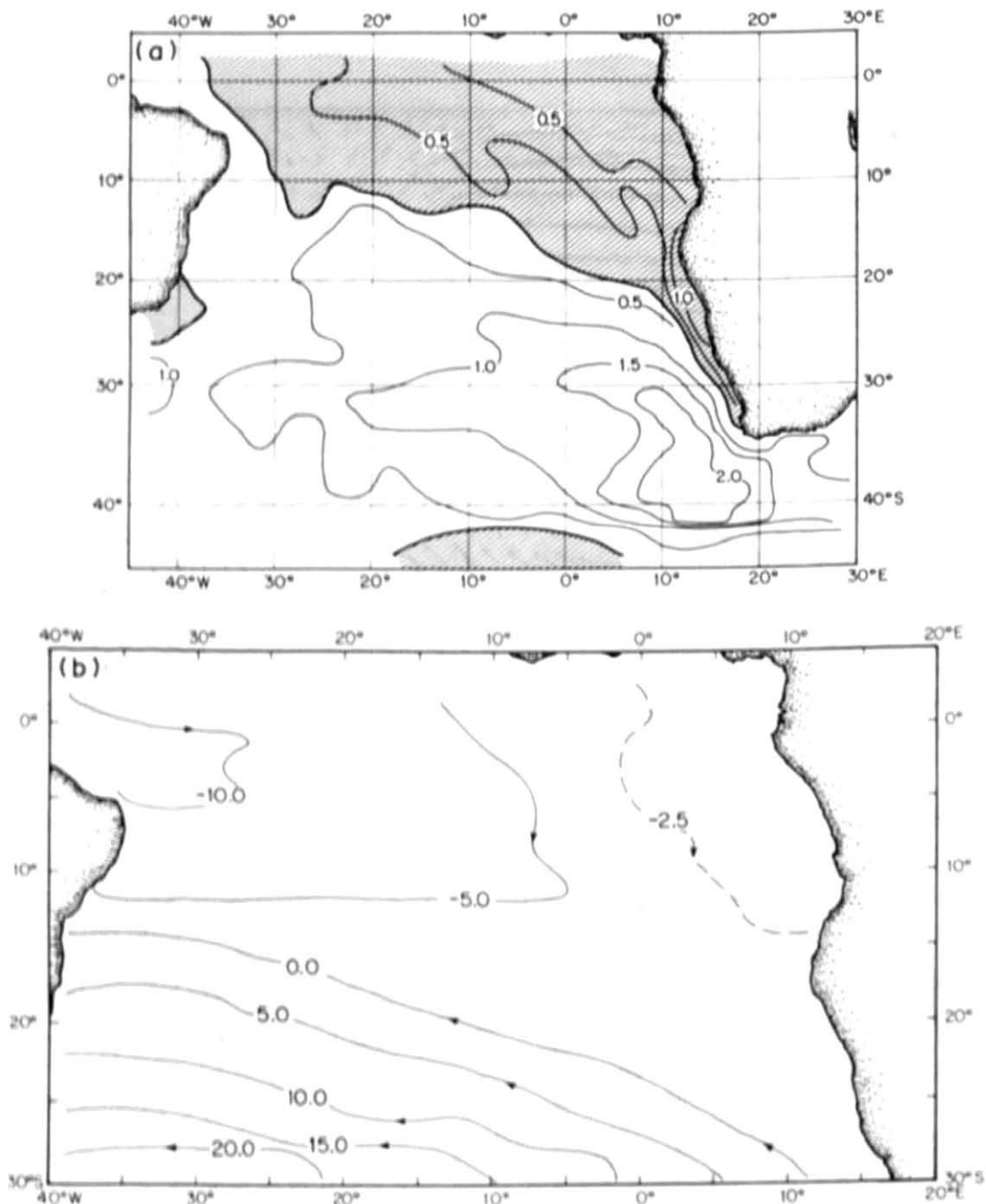
10 cm/sec

Fig. 6.   (c) and (d).

Fig. 7. (a) Curl of the mean annual wind stress in 10^{-7} N m^{-1}. Values of wind stress are from HELLERMAN and ROSENSTEIN (1983). Regions of negative curl are hatched. (b) Sverdrup transport streamfunction from the eastern boundary

(θ/S) relations for these sections (Fig. 8) define the regional water mass structure. The Ajax θ/S relation (Fig. 8a) clearly shows the two basic thermocline regimes on either side of the Angola–Benguela Front, falling at 18°S (between Ajax Stas 25 and 26, a distance of 110 km apart). The salinity change across the front averages 0.1 psu within the thermocline, with higher salinity in the cyclonic gyre. Differences in salinity diminish with depth. The cyclonic gyre water column remains more saline well into the deep water, at least to 2.5°C, though the frontal structure disappears.

At temperatures warmer than approximately 17°C the waters within the cyclonic gyre display a varied θ/S structure. The stations north of 8°S (Stas 10–16) have a nearly 35.8

isohaline structure above 17°C. South of 10°S, Stas 20–25 (which include the center of the gyre and its southern limb) show increasing salinity with increasing temperature, a situation found across the western limb of the gyre into the western South Atlantic (Fig. 8b). The isohaline layer is equatorial water, induced as upwelled water is heated. The
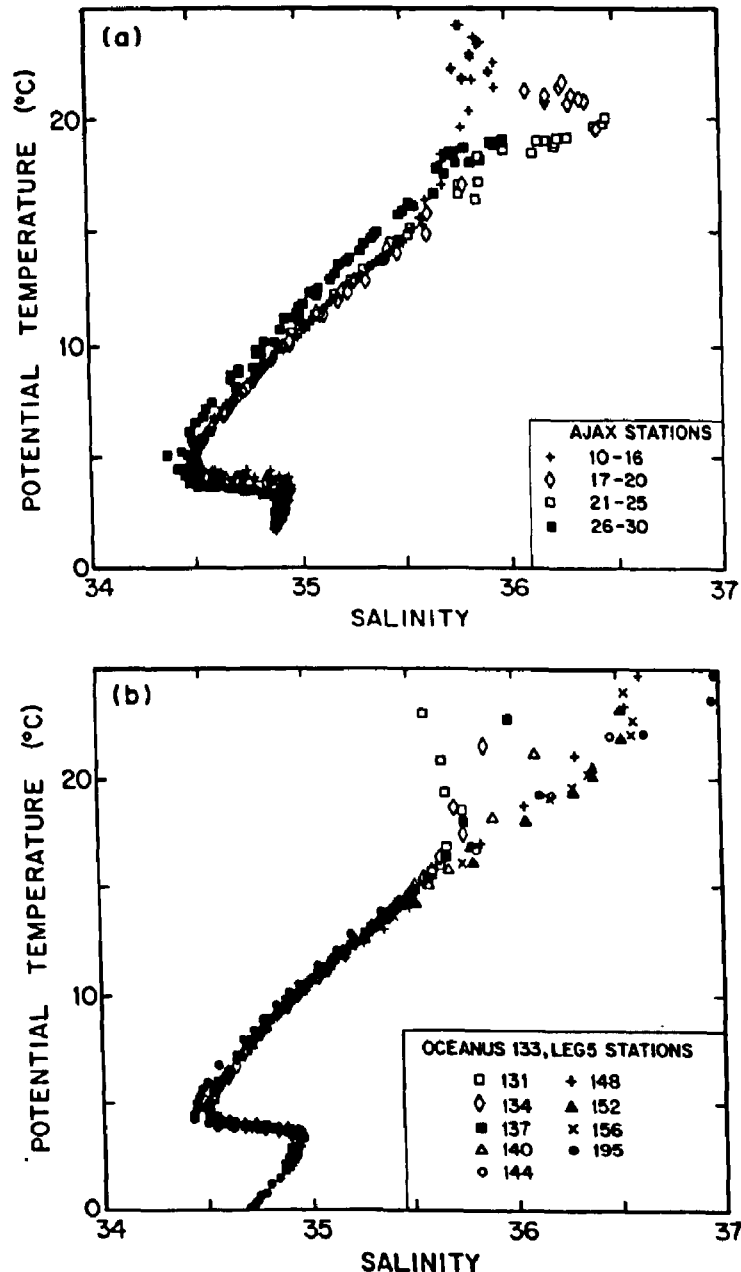

Fig. 8. (a) θ/S along the Greenwich Meridian: 1.5°–7.5°S (Ajax Stas 10–16, marking the equatorial limb of the cyclonic gyre); 8.6°–12°S (Ajax Stas 17–20, marking the region immediately north of the gyre center); 13°–17°S (Ajax Stas 21–25, marking the center and southern limb of the cyclonic gyre); and 18°–22°S (Ajax Stas 26–30, within the Benguela Current south of the cyclonic gyre). The Angola–Benguela Front falls between groupings 21–25 and 26–30. (b) θ/S along 11°S using select stations from R.V. Oceanus 11°S cruise (Fig. 2). Stations 131–144 are within the eastern limb of the cyclonic gyre, the Angola Current. Stations 148–156 mark the gyre's western limb. Station 195 is within the western boundary of the South Atlantic.
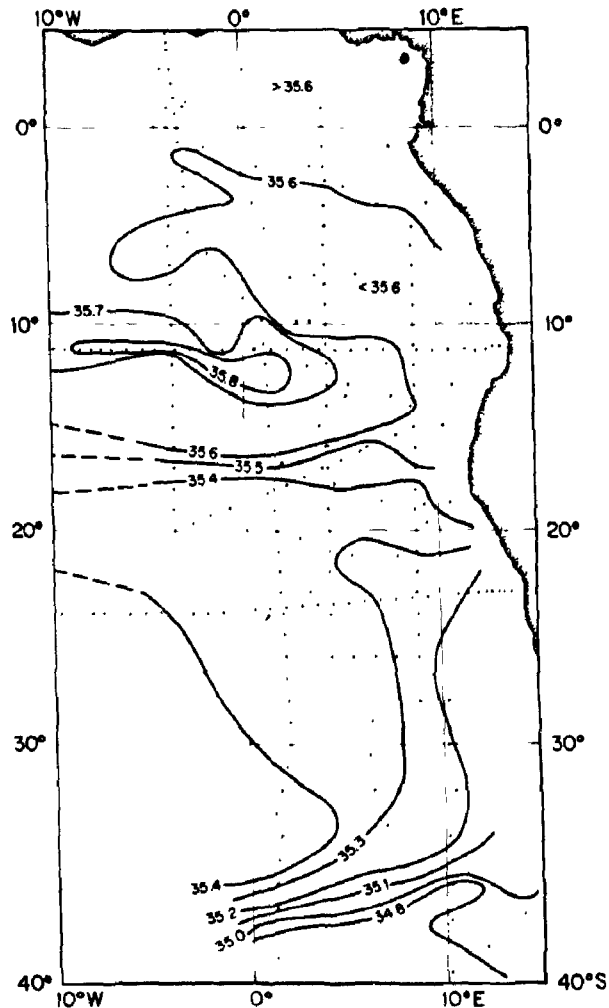
Fig. 9. Salinity on σ_θ surface 26.3 (upper part of the thermocline).

more saline surface water to the south is subtropical surface water. Between 8° and 10°S (Stas 17–20) the surface water appears to be a mix of equatorial and subtropical water.

The R.V. *Oceanus* 11°S θ/S relation (Fig. 8b) at temperatures below 17°C displays a tight envelope of points within the cyclonic gyre. Station 195 in the western Atlantic is lower in salinity within the lower thermocline and Antarctic Intermediate Water, as expected, since it derives water from the subtropical gyre and is fed directly by the source of Antarctic Intermediate Water in the southwest Atlantic (PIOLA and GORDON, 1989). Above 17°C the R.V. *Oceanus* data reflect the same structure observed within the Ajax data. The isohaline layer above 17°C occurs in the eastern limits marking the Angola Current, as it draws water from the equatorial regime to the north, while within the center part and western branch of the gyre the surface water is of the salty subtropical variety. The surface salinity in the eastern boundary is lower in salinity than the equatorial water, a condition that probably reflects the addition of fresh water by the Congo River discharge.

A map view of the Angola–Benguela Front within the thermocline is provided by a plot of salinity on the $\sigma_\theta = 26.3$ density surface, which ranges in depth from less than 75 m to greater than 200 m (Fig. 9). A strong meridional salinity gradient near 18°S marks the Angola–Benguela Front, and a high salinity core is observed within the gyre center.

The Angola–Benguela Front is particularly striking in θ/O_2 space (Fig. 10). The water north of the front, within the cyclonic gyre, is lower in O_2 concentration by as much as 3 ml l^{-1} at temperatures between 8 and 17°C. Stations 26 and 27 represent a reversal in the meridional oxygen gradient, as also seen by the salinity contrast on the θ/S plot (Fig. 8a). This reflects an eddy or meander in the front. Inspection of the R.V. *Oceanus* oxygen data along 11°S indicates a strongly depleted oxygen concentration (<1 ml l^{-1}) within the eastern limb of the cyclonic gyre. The oxygen data shown by CHAPMAN and SHANNON (1987) show oxygen-depleted waters within the cyclonic gyre region throughout the year. These waters are thought to be a product of the high productivity region off Angola (MAZEIKA, 1967; VOITURIEZ and HERBLAND, 1982).

Intermediate and deep water masses

Below the thermocline are Antarctic Intermediate Water (AAIW) marked by the salinity minimum (Fig. 11a) and the North Atlantic Deep Water (NADW) marked by a deep salinity maximum (Fig. 11b).

At the AAIW stratum the salinity within the cyclonic gyre region is significantly above that of the western South Atlantic (R.V. *Oceanus* Sta. 195) where concentrated AAIW spreads northward. Within the eastern extent there is minor salinity variation: slightly higher salinity values are observed within AAIW in the easternmost stations. These values are higher than those found in the Ajax stations south of the Angola–Benguela Front, as well as those within the northern limb of the cyclonic gyre. This is also shown by KIRWAN (1963), who on inspecting isopycnal surfaces at and near the AAIW stratum, concludes: "The presence of the northern clockwise gyral indicates a considerable amount of return flow along the eastern boundary of the South Atlantic." It is suggested that the slightly more saline AAIW in the region of the cyclonic gyre is a product of vertical mixing, which would transfer salty thermocline water characteristic into the AAIW stratum.

The NADW salinity maximum (Fig. 11b) at the African margin is significantly saltier than that of the interior (though less than the salinity maximum at R.V. *Oceanus* Sta. 195 of the western South Atlantic, marking the main path of the southward spreading of
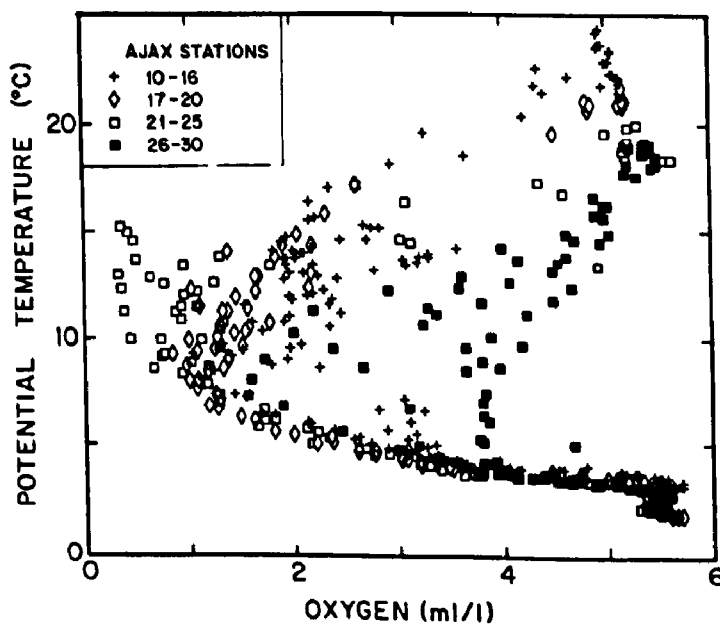

Fig. 10. θ/O_2 along the Greenwich Meridian using the same stations as used in Fig. 8a.
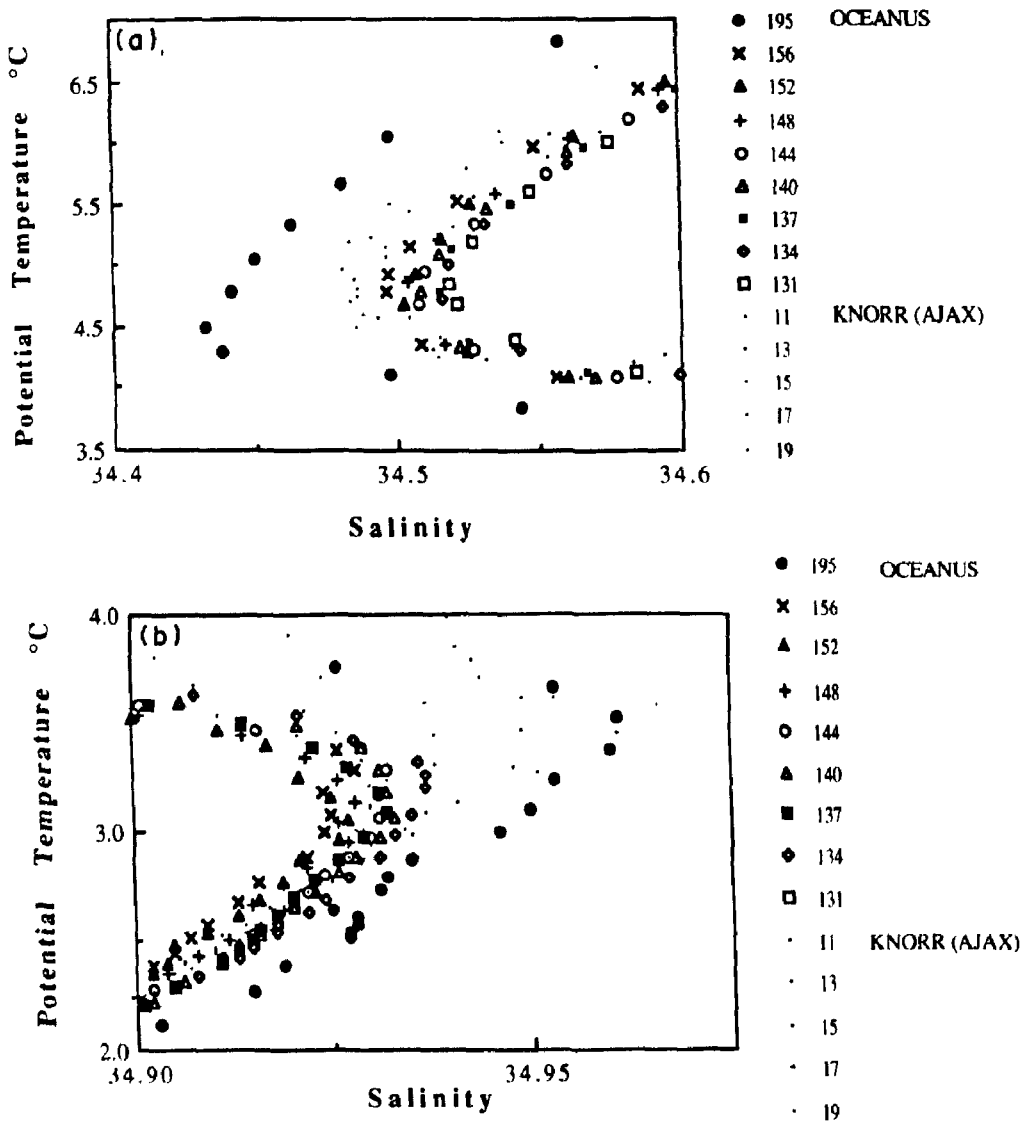
Fig. 11. (a) θ/S at the salinity minimum of the Antarctic Intermediate Water, using the same R.V. *Oceanus* stations as used in Fig. 8b and characteristic stations from the two northern Ajax station groups used in Fig. 8a. (b) θ/S at the salinity maximum of the North Atlantic Deep Water, using the same stations as used in (a).

NADW). The salinity maximum in the eastern end of the R.V. *Oceanus* section (Sta. 134) is only slightly below that observed within the equatorial region of the Ajax data. A salinity maximum core layer map for the eastern South Atlantic based on the 1983–1984 data set (Fig. 12) portrays a slight preference for poleward deflection of the isohalines near the eastern boundary, south of 10°S. This extends to at least 30°S. Possibly NADW spreading along the eastern boundary in the South Atlantic is derived from the equatorial region, where branching of NADW from the western boundary is reported (WEISS *et al.*, 1985).

The eastern spreading path of the NADW salinity maximum is puzzling; is it consistent with the abyssal circulation model of STOMMEL and ARONS (1960)? WARREN and SPEER (1991) address this issue. Using a Stommel and Arons model tailored to the geometry of the Angola Basin at a depth of the NADW, they predict a deep, broad poleward flow of saline NADW along the eastern boundary. The salinity maximum core layer map (Fig. 12)
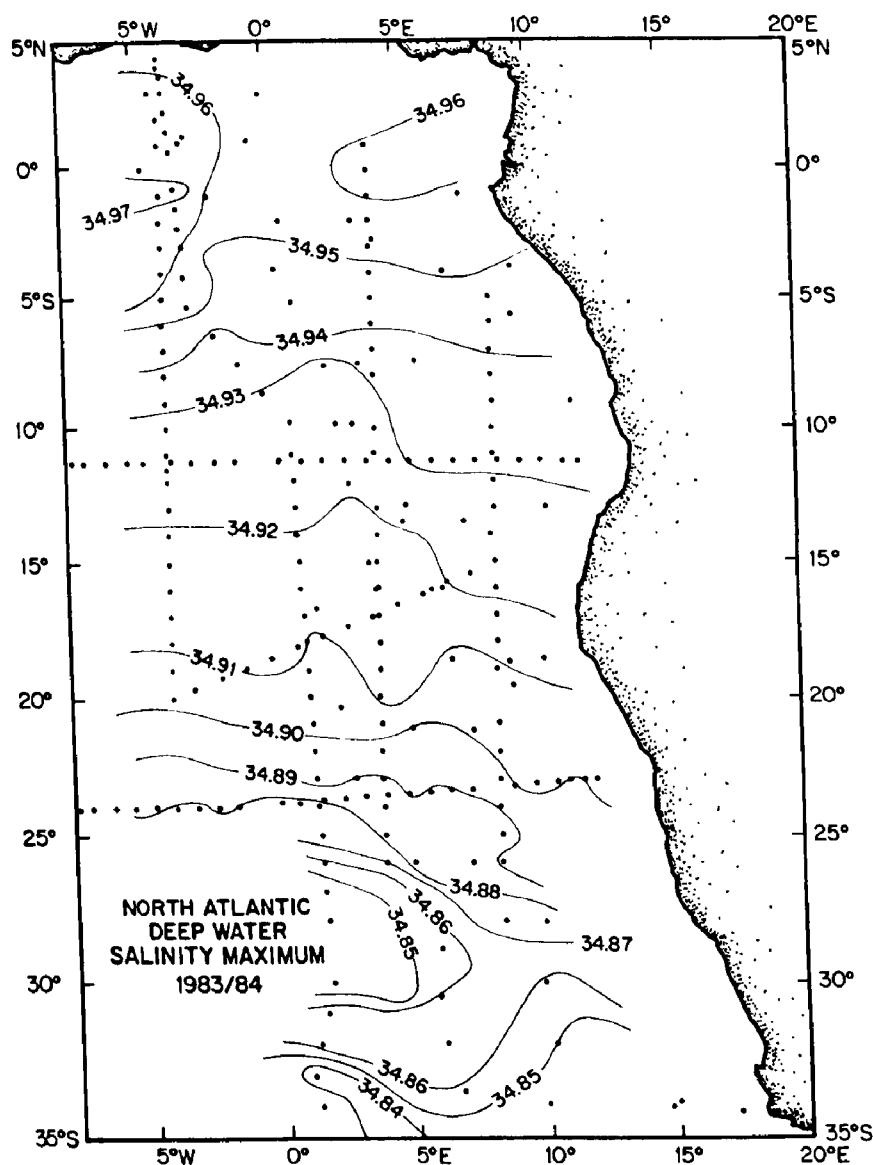
Fig. 12.   Salinity maximum core layer map marking the North Atlantic Deep Water using the
1983–1984 station array shown in Fig. 2.

suggests that the null point (the point where two opposing western boundary currents meet; Warren and Speer arbitrarily match the strength of the opposing boundary currents) is at 10°S rather than 20°S as shown by Warren and Speer. Additionally, consideration of linear wave (e.g. Kelvin waves) propagation may be needed. Kelvin waves are generated in the equatorial region and propagate eastward along the equatorial wave guide. Upon reaching the eastern boundary they are expected to move poleward along the coastline (GILL, 1982; KAWASE, 1987).

Thermocline residence time

The origin of the thermocline water within the cyclonic gyre is most likely from the south. The southern extent of the salty North Atlantic thermocline is well north of the equator (BROECKER and TAKAHASHI, 1981) and does not feed the eastward-flowing

components of the equatorial circulation. The North Equatorial Countercurrent is derived from the South Equatorial Current, a South Atlantic thermocline structure (Richardson and Reverdin, 1987) and the Equatorial Undercurrent is also derived from the South Atlantic thermocline (Metcalf and Stalcup, 1967). The geostrophic circulation of the sea surface and 500 db surface relative to 1500 db (Fig. 3) indicates that the water within the cyclonic gyre is derived from inflow from the west, which in turn is drawn from the water flowing from the southeast South Atlantic as part of the subtropical anticyclonic gyre. It is suspected that the salty thermocline of the cyclonic gyre results from the regional excess evaporation. A residence time can be determined: how long does it require to convert the water column of the southeast South Atlantic to that of the cyclonic gyre? In the following calculations, the water columns as observed during the Ajax expedition on either side of the Angola–Benguela Front are used for initial and final conditions.

A map of precipitation minus evaporation indicates that the entire South Atlantic from the equator to 40°S is a region where evaporation exceeds precipitation (Baumgartner and Reichel, 1975). Using an evaporation–precipitation rate of $1.2 \, \mathrm{m \, y^{-1}}$ (Baumgartner and Reichel, 1975) and assuming that the excess salt is distributed over the upper 300 m (the depth to which there is a significant salinity difference across the Angola–Benguela Front), a gyre residence time of 1.0 years is required to account for the salinity difference of 0.14 psu (determined from comparison of Ajax Stas 21 and 28 marking the center of the gyre and the water south of the Angola–Benguela Front, respectively).

A more appropriate evaluation of residence time within the gyre would include continental run-off. Reduced surface salinity over much of the eastern extent of the cyclonic gyre attests to the importance of the river discharge to the local water balance. The Congo River is the second largest river in the world in terms of annual discharge. It discharges approximately $1.4 \times 10^{12} \, \mathrm{m^3 \, y^{-1}}$ into the South Atlantic just south of 5°S (Dongey et al., 1965). If the total annual Congo output is averaged over the estimated area of the gyre and to the depth of 300 m, the residence time within the gyre increases from 1.0 to 4.4 years. If all of the rivers that drain into the Angola Basin were included (1.6×10^{12} $\mathrm{m^3 \, y^{-1}}$, Jean-Marc Verstraete, personal communication, 1989), the residence time increases to 8.5 years. In view of uncertainties in the fresh-water distribution within the gyre, a residence time of 4–10 years is suggested.

In consideration of the oxygen deficit within the cyclonic gyre of $2.2 \, \mathrm{ml \, l^{-1}}$ (using the same two Ajax stations used from the salinity difference determinations for the depth range from 100 m, below the surface layer, to 300 m), the 4.4 year residence time calculated with Congo River input yields $0.5 \, \mathrm{ml \, l^{-1} \, y^{-1}}$ for oxygen utilization. Consideration of all river input reduced oxygen utilization to $0.3 \, \mathrm{ml \, l^{-1} \, y^{-1}}$. An investigation of in situ oceanic oxygen utilization of Subtropical Mode Water within the Sargasso Sea gave a value of $0.20 \pm 0.02 \, \mathrm{ml \, l^{-1} \, y^{-1}}$ (Jenkins, 1977). The Sargasso Sea region is not a highly productive area. Given the signs of enhanced productivity within the eastern margins of the tropical South Atlantic (Voituriez and Herbland, 1982), an oxygen consumption rate between 0.3 and $0.5 \, \mathrm{ml \, l^{-1} \, y^{-1}}$ appears reasonable.

DISCUSSION

The baroclinic circulation pattern presented by the 1983–1984 data compares reasonably well with that of Moroshkin et al. (1970) and the climatic mean pattern as revealed by

the Levitus gridded data set. The circulation within the eastern tropical South Atlantic Ocean is one of a weak, but climatically stationary, cyclonic gyre. The baroclinic representation of the gyre is most pronounced within the upper 300 db, camouflaged in the surface layer by the Ekman flow. Current observations of poleward flow along the coast of Gabon provide compelling direct evidence of the eastern limb of this cyclonic gyre (WACONGNE, 1988). At the depth of the NADW stratum there appears to be a slight preference for southward spreading along the eastern boundary.

Cyclonic circulation features and thermal domes have been observed in the eastern margins of other tropical oceans, although the South Atlantic example seems to be best defined. During the northern hemisphere summer a thermal dome (Guinea Dome) forms southwest of Dakar in the North Atlantic (ROSIGNAL and MEYRUEIS, 1964; MAZEIKA, 1967). The Costa Rica Dome is a feature of the North Pacific (WYRTKI, 1964), centered at 7°–8°N. Though smaller, it exhibits many similarities to the cyclonic gyre in the South Atlantic. The North Equatorial Countercurrent approaches the coast of Central America and then turns north as the Costa Rica Current. This is analogous to the South Equatorial Countercurrent and the Angola Current of the South Atlantic. The Costa Rica Dome also exhibits high salinity surface water in the gyre center and very low thermocline oxygen values, as does the South Atlantic cyclonic gyre. Both of the cyclonic circulation patterns attenuate rapidly with depth.

The North Equatorial Countercurrents are more established in the North Atlantic and North Pacific tropical oceans than is the South Equatorial Countercurrent, and cyclonic gyres are visible in the dynamic topography of these oceans (North Pacific, REID and MANTYLA, 1978; North Atlantic, REID, 1978). Although there is no mean cyclonic gyre in the South Pacific, a warm southward-flowing current similar to the Angola Current is evident along the coast of Peru during El Niño years (CANE, 1986). The eastern tropical South Indian Ocean is unique in view of its strong monsoonal forcing and interaction with the Indonesian throughflow. The dynamic topography maps of WYRTKI (1971) indicate a cyclonic gyre centered in the western tropical South Indian Ocean, with a much smaller cyclonic gyre immediately south of Java during the summer monsoon (June–November; see WYRTKI, 1971).

REFERENCES

ARNAULT S. (1987) Tropical Atlantic geostrophic currents and ship drifts. Journal of Geophysical Research, 92, 5076–5088.

BAUMGARTNER A. and E. REICHEL (1975) The world water balance. Elsevier Science Publishers, New York, 179 pp.

BROECKER W. S. and T. TAKAHASHI (1981) Hydrography of the central Atlantic—IV. Intermediate waters of Antarctic origin. Deep-Sea Research, 28, 177–193.

CAMP D., W. HAINES, B. HUBER, S. RENNIE and A. GORDON (1986) Agulhas Retroflection Cruise, Lamont-Doherty Technical Report LDGO-86-1.

CANE M. A. (1986) El Niño. Annual Review of Earth and Planetary Science, 14, 43–70.

CHAPMAN P. and L. V. SHANNON (1987) Seasonality in the oxygen minimum layers at the extremities of the Benguela System. In: The Benguela and comparable ecosystems, A. I. L. PAYNE, J. A. GULLAND and K. H. BRINK, editors, South African Journal of Marine Science, 5, 85–94.

CURRIE R. (1953) Upwelling in the Benguela Current. *Nature*, 171, 497–500.

DEFANT A. (1961) *Physical oceanography*, Vol. 1, Pergamon Press, Oxford, 729 pp.

DONGEY J. R., J. HARDIVILLE and J. C. LeGUEN (1965) Le parcours maritime des eaux du Congo. *Cahiers Oceanographiques*, 17, 85–97.

GILL A. E. (1982) *Atmosphere–ocean dynamics*. International Geophysics Series, 30, Academic Press, New York, 662 pp.

GORDON A. L. (1965) Quantitative study of the dynamics of the Caribbean Sea. Ph.D. Thesis, Columbia University, New York, 233 pp.

HART T. J. and R. I. CURRIE (1960) The Benguela Current. Discovery *Report*, 31, 123–298.

HASTENRATH S. and P. J. LAMB (1977) *Climatic atlas of the tropical Atlantic and eastern Pacific Oceans*, University of Wisconsin Press, Madison, 15 pp., 97 charts.

HASTENRATH S. and J. MERLE (1987) Annual cycle of subsurface thermal structure in the tropical Atlantic Ocean. *Journal of Physical Oceanography*, 17, 1518–1531.

HELLERMAN S. and M. ROSENSTEIN (1983) Normal monthly wind stress over the world ocean with error estimates. *Journal of Physical Oceanography*, 13, 1093–1104.

HORTON C. and W. STURGES (1979) A geostrophic comparison during MODE. *Deep-Sea Research*, 26, 521–533.

JENKINS W. J. (1977) Tritium–helium dating in the Sargasso Sea: a measurement of oxygen utilization rates. *Science*, 196, 291–292.

KAWASE M. (1987) Establishment of deep ocean circulation driven by deep water production. *Journal of Physical Oceanography*, 17, 2294–2317.

KIRWAN A. D. (1963) Circulation of Antarctic intermediate water deduced through isentropic analysis. Texas A&M technical report, Ref. 63-34 F, 34 pp, 47 Figures.

LEGICKIS (1989) Cover of *Eos*, 70 (2).

LEVITUS S. (1982) Climatological atlas of the world ocean, NOAA Professional Paper 13, U.S. Government Printing Office, Washington, DC.

MAZEIKA P. A. (1967) Thermal domes in the Eastern Tropical Atlantic Ocean. *Limnology and Oceanography*, 12, 537–539.

MAZEIKA P. A. (1968) The marine environment, Folio 16, American Geophysical Society, New York.

MERLE J. (1978) Atlas hydrologique saisonnier de l'ocean Atlantique. Travaux et Documents de l'O.R.S.T.O.M, no. 82, 185 pp.

METCALF W. G. and M. C. STALCUP (1967) Origin of the Atlantic Equatorial Undercurrent. *Journal of Geophysical Research*, 72, 4959–4975.

MOLINARI R. L. (1982) Observations of eastward currents in the tropical South Atlantic Ocean: 1978–1980. *Journal of Geophysical Research*, 87, 9707–9714.

MOLINARI R. L., B. VOITURIEZ and P. DUNCAN (1981) Observations in the subthermocline undercurrent of the Equatorial South Atlantic Ocean: 1978–1980. *Oceanologica Acta*, 4, 451–456.

MOROSHKIN K. V., V. A. BUBNOV and R. P. BULATOV (1970) Water circulation in the eastern South Atlantic Ocean. *Oceanology*, 10, 27–34.

PHILANDER S. G. H. and R. C. PACANOWSKI (1986) A model of the seasonal cycle in the Tropical Atlantic Ocean. *Journal of Geophysical Research*, 91, 14,192–14,206.

PIOLA A. R. and A. L. GORDON (1989) Intermediate Water in the southwestern South Atlantic. *Deep-Sea Research*, 36, 1–16.

POND S. and G. L. PICKARD (1983) *Introductory dynamical oceanography*, Pergamon Press, Oxford 329 pp.

PRICE J. F., R. A. WELLER and R. R. SCHUDLICH (1987) Wind-driven ocean currents and Ekman transport. *Science*, 328, 1534–1538.

REID J. L. (1964) Evidence of a South Equatorial Countercurrent in the Atlantic Ocean in July 1963. *Nature*, 203, 1182.

REID J. L. (1978) On the mid depth circulation and salinity field in the North Atlantic Ocean. *Journal of Geophysical Research*, 83, 5063–5067.

REID J. L. and A. W. MANTYLA (1978) On the mid depth circulation of the North Pacific Ocean. *Journal of Physical Oceanography*, 8, 946–951.

REID J. L., W. D. NOWLIN and W. C. PATZERT (1977) On the characteristics and circulation of the Southwestern Atlantic Ocean. *Journal of Physical Oceanography*, 7, 62–91.

RICHARDSON P. L. (1988) Historical Shipdrift. SAARI report, Lamont-Doherty Geological Observatory, Palisades, New York, 67 pp.

RICHARDSON P. L. and D. WALSH (1986) Mapping climatological seasonal variations of surface currents in the Tropical Atlantic using ship drifts. *Journal of Geophysical Research*, **91**, 10,537–10,550.

RICHARDSON P. L. and S. G. H. PHILANDER (1987) The seasonal variations of surface currents in the tropical Atlantic Ocean: a comparison of ship drift data with results from a general circulation model. *Journal of Geophysical Research*, **92**, 715–724.

RICHARDSON P. L. and G. REVERDIN (1987) Seasonal cycle of velocity in the Atlantic North Equatorial Countercurrent as measured by surface drifters, current meters and ship drifts. *Journal of Geophysical Research*, **92**, 3691–3708.

ROSIGNAL M. and A. M. MEYRUEIS (1964) Campagne oceanographique de Gerard-Treca. Office Rech. Sci. Tech. Outre-Mer, Centre Oceanog, Dakar-Thiaroye, 53 pp.

SHANNON L. V. (1985) The Benguela ecosystem. 1. Evolution of the Benguela, physical features and processes. In: *Oceanography and marine biology. An annual review*, Vol. 23, M. BARNES, editor, Aberdeen University Press, pp. 105–182.

SHANNON L. V., A. J. BOYD, G. B. BRUNDRIT and J. TAUNTON-CLARK (1986) On the existence of El Niño-type phenomenon in the Benguela system. *Journal of Marine Research*, **44**, 495–520.

SHANNON L. V., J. J. AGENBAG and M. E. L. Buys (1987) Large and mesoscale features of the Angola–Benguela front. In: *The Benguela and comparable ecosystems*, A. I. L. PAYNE, J. A. GULLAND and K. H. BRINK, editors, *South African Journal of Marine Science*, **5**, 11–34.

SIO (1985) Physical, chemical and *in situ* CTD data from the Ajax Expedition aboard R. V. *Knorr*. SIO Ref. 85-24, 274 pp.

STOMMEL H. and A. B. ARONS (1960) On the abyssal circulation of the world ocean—I. Stationary planetary flow patterns on a sphere. *Deep-Sea Research*, **6**, 140–154.

SVERDRUP H. U. (1947) Wind-driven currents in a baroclinic ocean; with application to the equatorial currents of the eastern Pacific. *Proceedings of the National Academy of Science*, **33**, 318–326.

SWALLOW J. (1977) An attempt to test the geostrophic balance using mini-mode current measurements. In: *A voyage of Discovery*, M. ANGEL, editor, Pergamon Press, Oxford, pp. 165–176.

TSUCHIYA M. (1985) Evidence of a double-cell subtropical gyre in the South Atlantic Ocean. *Journal of Marine Research*, **43**, 57–65.

VOITURIEZ B. and A. HERBLAND (1982) Comparaison des systèmes productifs de l'Atlantique Tropical Est: dômes thermiques, upwellings côtiers et upwelling equatorial. *Rapports et Proces-Verbaux des Reunions. Conseil Permanent International pour l'Exploration de la Mer*, **180**, 114–130.

WACONGNE S. (1988) Dynamics of the Equatorial Undercurrent and its termination. Ph.D. Thesis, MIT/WHOI, WHOI-88-10.

WARREN B. A. and K. G. SPEER (1991) Deep circulation in the eastern South Atlantic Ocean. *Deep-Sea Research*, **38** (Suppl.), S281–S322.

WEISS R. F., J. L. BULLISTER, R. H. GAMMON and M. J. WARNER (1985) Atmospheric chlorofluoromethanes in the deep equatorial Atlantic. *Nature*, **314**, 608–610.

WÜST G. (1924) Florida-Antllenstrom. *Veroffentichungen des Institutes fur Meereskunde an der Universitat*, Berlin, **12**, 48 pp.

WYRTKI K. (1964) Upwelling in the Costa Rica Dome. *U.S. Fish Wildlife Service, Fisheries Bulletin*, **63**, 355–371.

WYRTKI K. (1971) *Oceanographic Atlas of the International Indian Ocean Expedition*. National Science Foundation, 531 pp.